The World Before Us

The New Science Behind Our Human Origins

TOM HIGHAM

Yale UNIVERSITY PRESS
New Haven & London

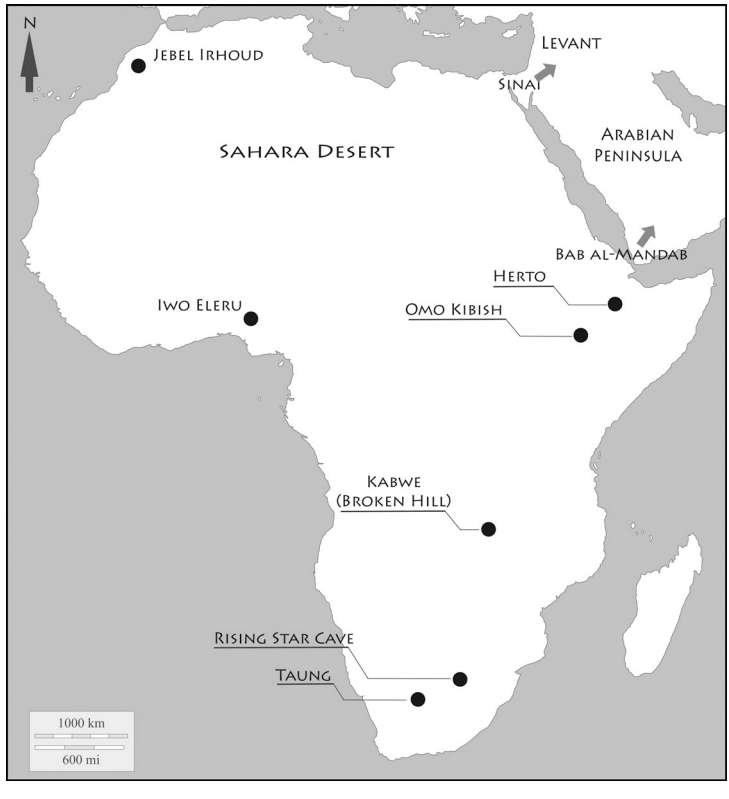

Figure 1 African sites and locations.

Figure 2 Mediterranean sites and locations.

Figure 3 The first of our kind. The earliest known *Homo sapiens* fossils, from the Jebel Irhoud site. These images are composites derived from micro-CT scans of multiple original fossils. The modern-looking face falls into the range of variation one sees in living humans, but there are archaic features in the braincase (shaded in the right hand image) suggesting that the shape of the brain had not yet reached that seen in modern humans.

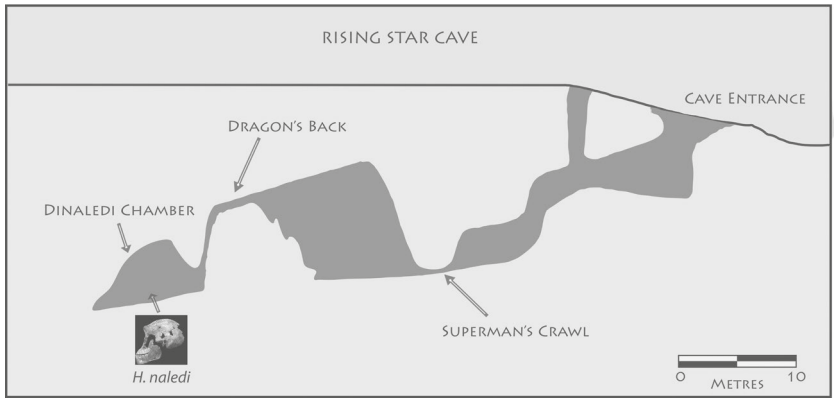

Figure 4 Plan of Rising Star Cave, with the location where the skeletal remains of *Homo naledi* were found.

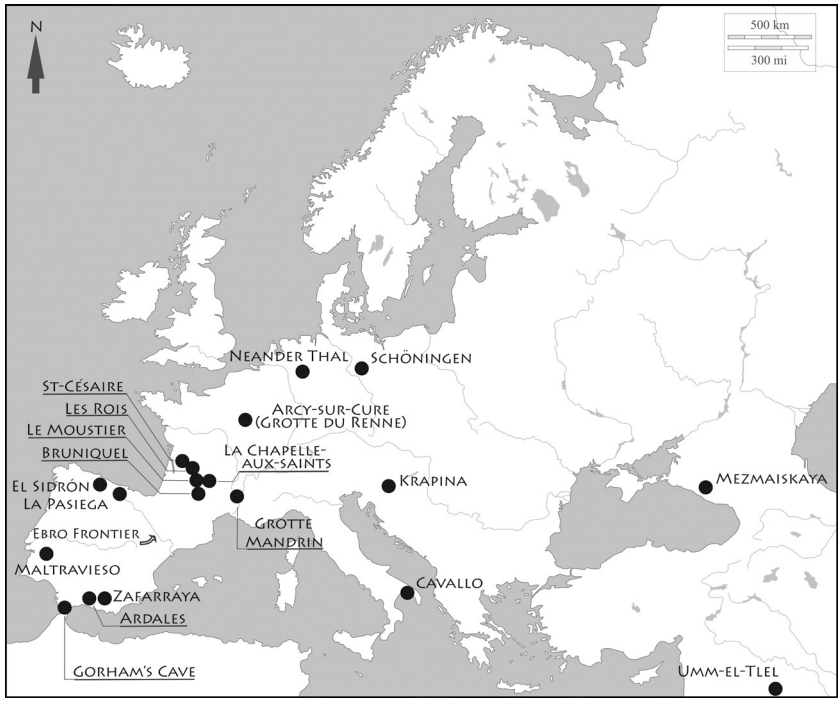

Figure 5 European and Near Eastern sites and locations.

Figure 6 A Neanderthal foot emerges from El Sidrón.

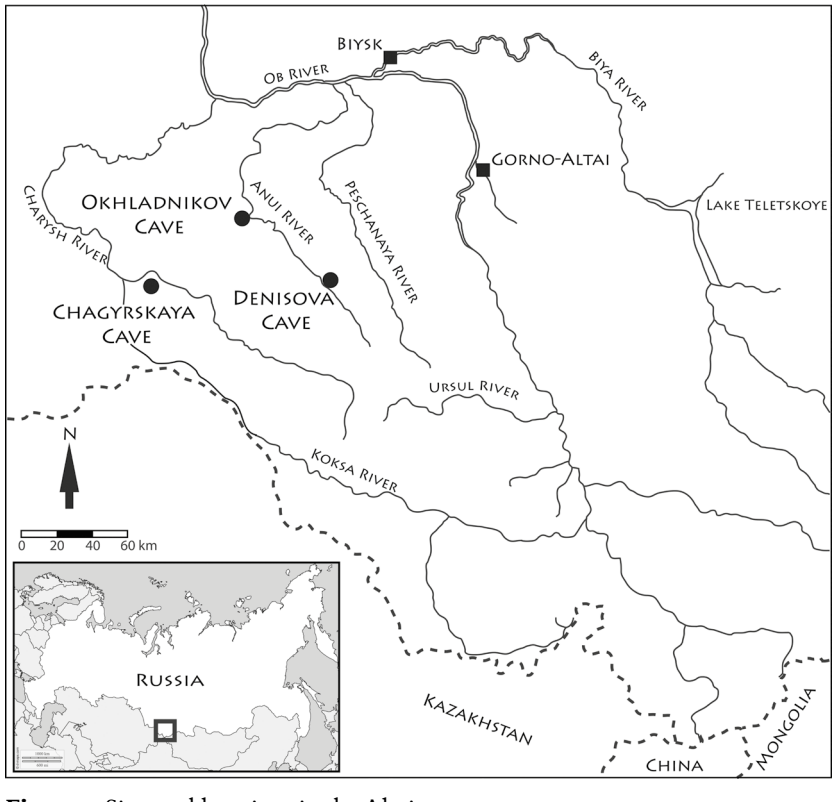

Figure 7 Sites and locations in the Altai.

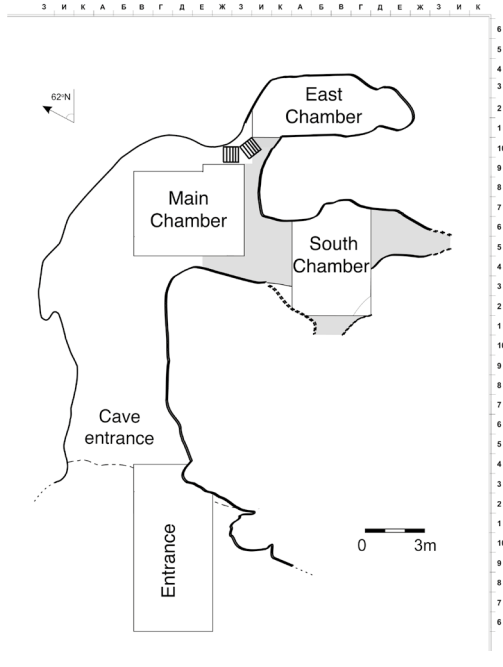

Figure 8 Plan of the different chambers and areas of excavation at Denisova Cave. The grey shaded areas are remaining sections of recent Holocene sediment.

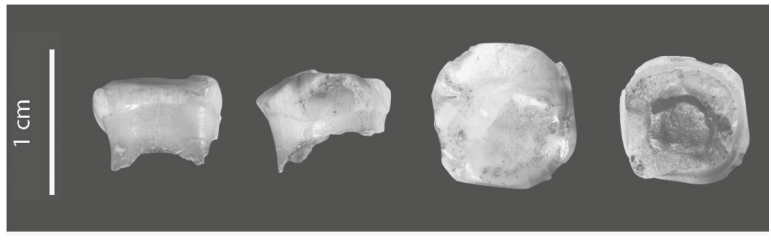

Figure 9 The Denisova 2 tooth, excavated in 1984 in the Main Chamber.

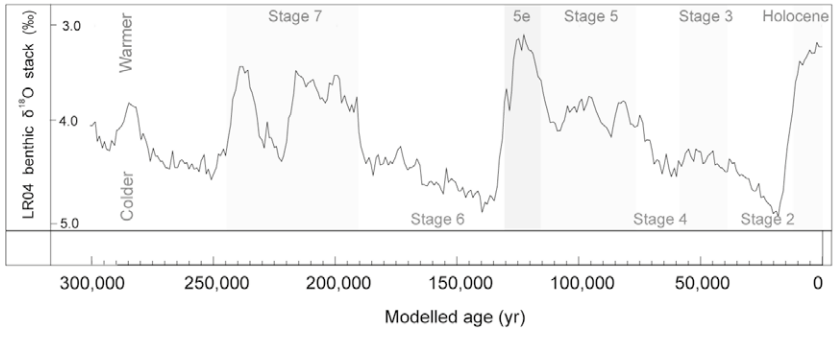

Figure 10 The record of climate change over the last 300,000 years based on oxygen isotope variations in marine foraminifera. The higher the peak, the warmer the temperature.

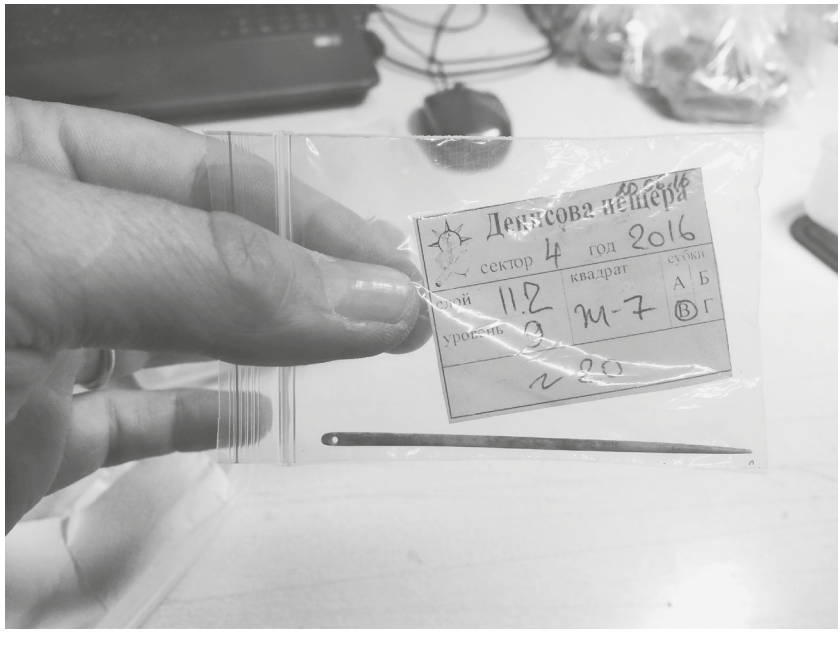

Figure 11 The author holding a plastic bag containing the recently excavated remains of a perfectly preserved bone needle from Denisova Cave.

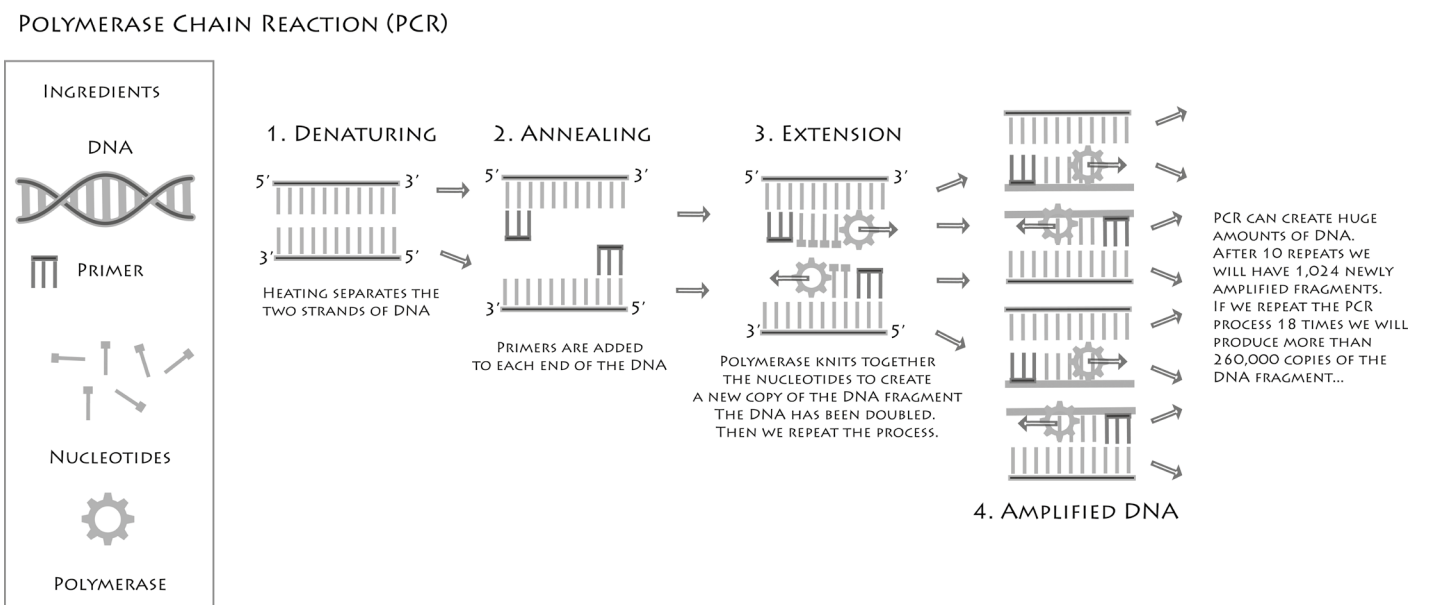

Figure 12 Schematic of the polymerase chain reaction.

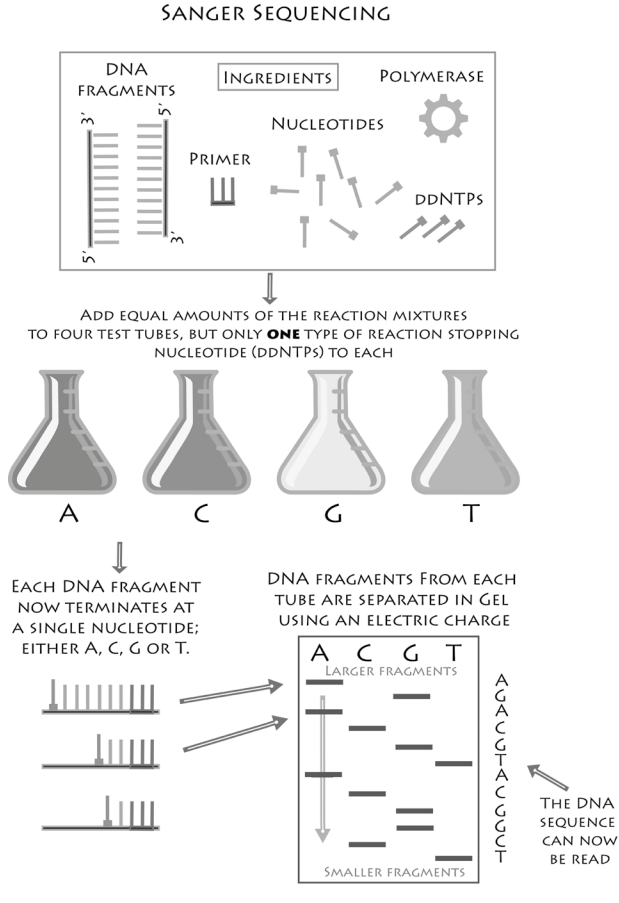

Figure 13 Schematic showing Sanger sequencing.

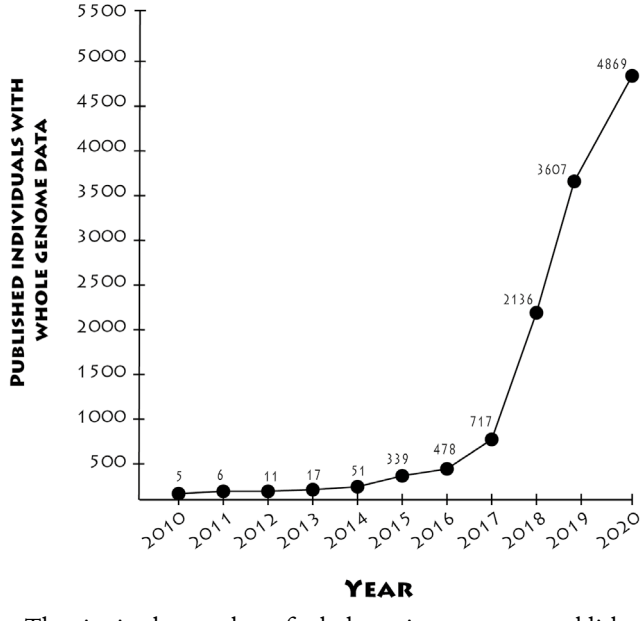

Figure 14 The rise in the number of whole ancient genomes published over the last decade, 2010–20 (note that 2020 figures are only for the first 6 months of the year) (data courtesy of David Reich, pers. comm.).

Figure 15 Far Eastern sites and locations.

Figure 16 Svante Pääbo (left) and the author at Denisova Cave in 2014.

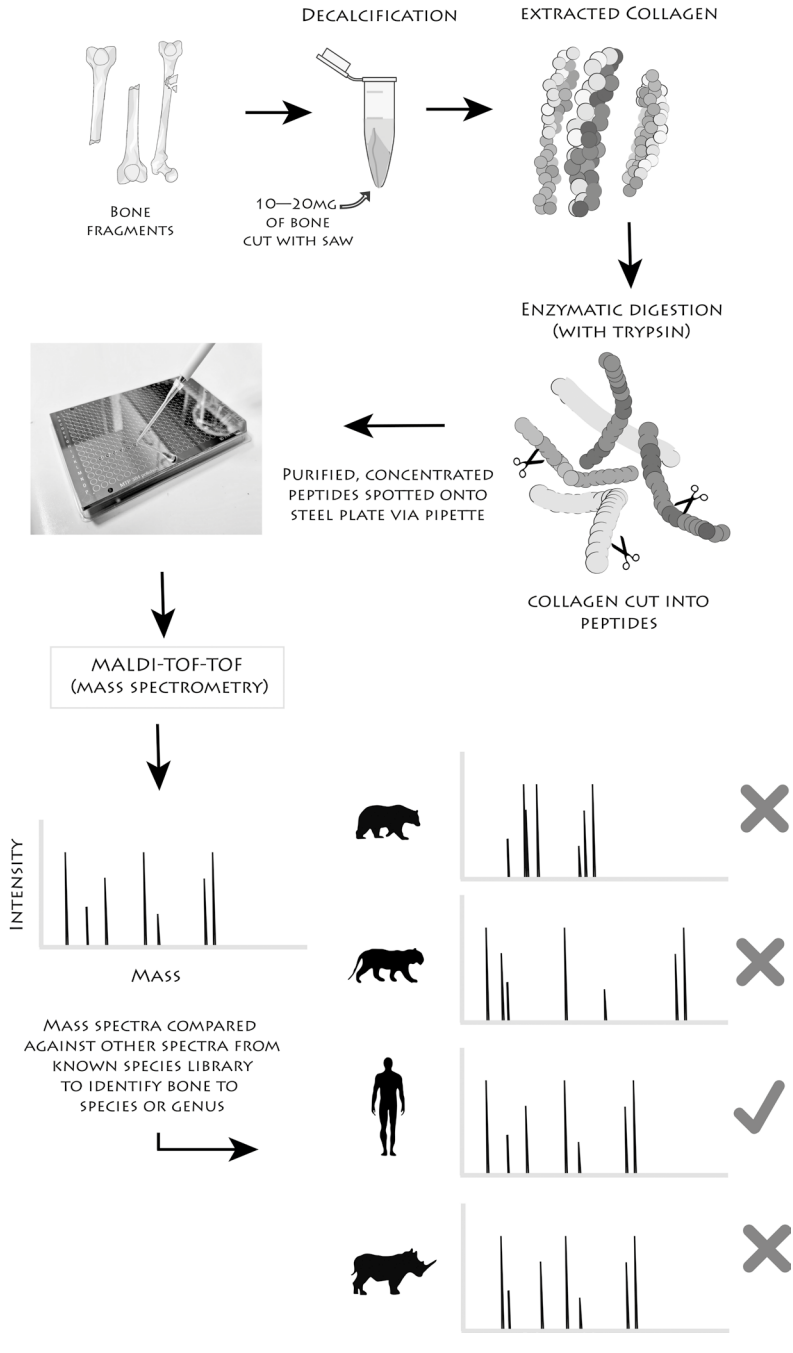

Figure 17 The method of using ZooMS to identify human bones.

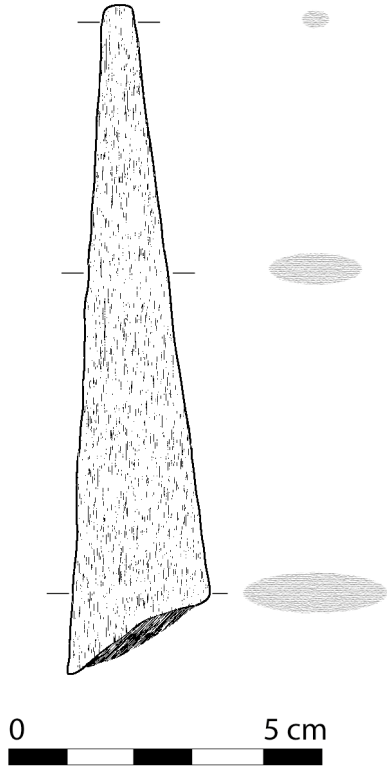

Figure 18 The Uphill bone point.

Figure 19 A perforated reindeer tooth pendant from Denisova Cave.

Figure 20 Keyhole sampling of a Denisovan tooth ornament.

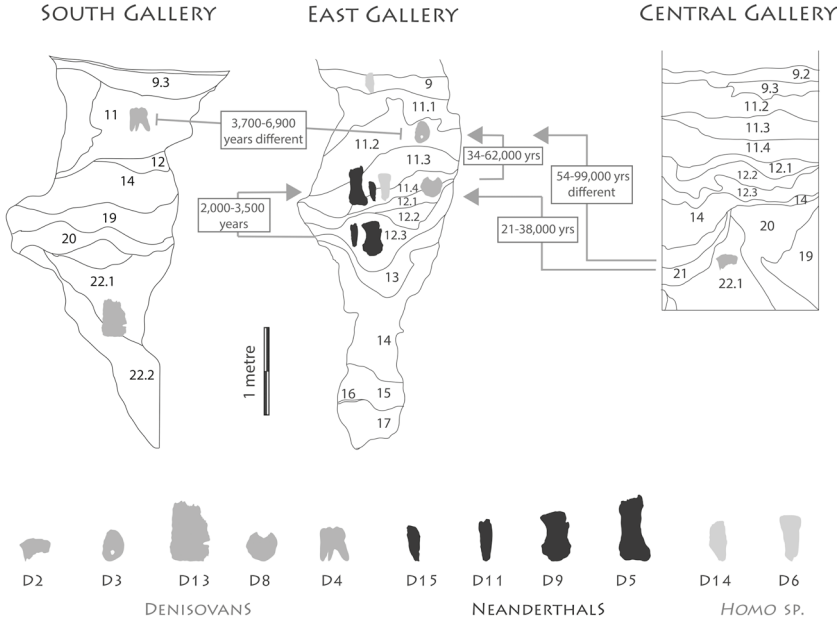

Figure 21 The basis of the Bayesian model we built. The excavated layers in each of the main chambers are shown. The silhouettes show the human remains of Denisovans and Neanderthals, as well as unidentified *Homo*. The lines show the age differences between the fossil bones as calculated using mitochondrial DNA analysis. The difference between Denisova 3 and 4, for example, was between 3,700 and 6,900 years. We used this to order the archaeological sequence relatively, from top to bottom. Radiocarbon and optical ages from the different layers were also used in the model.

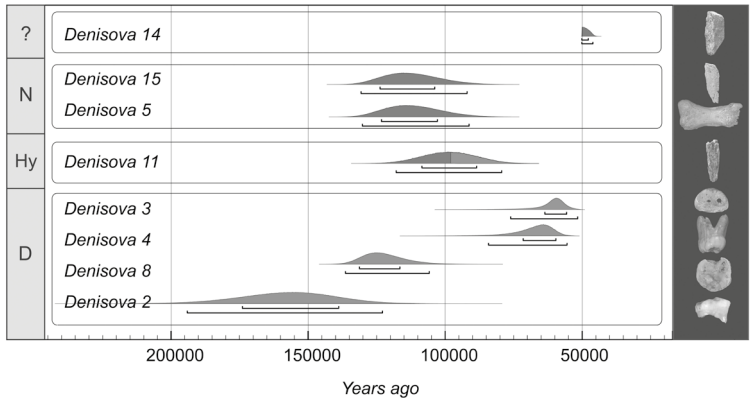

Figure 22 Final ages determined from Denisova Cave for all of the fossil remains. N = Neanderthals, D = Denisovans, Hy is, of course, Denny the hybrid, and the attribution for Denisova 14 is uncertain.

Figure 23 Distribution of Initial Upper Palaeolithic (IUP) sites across Eurasia and North Africa. T-P is Tenaghi Philippon.[1]

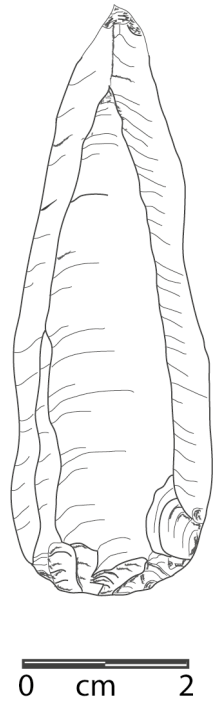

Figure 24 An Emiran point (redrawn after Belfer-Cohen and Goring-Morris 2017; see note 2).

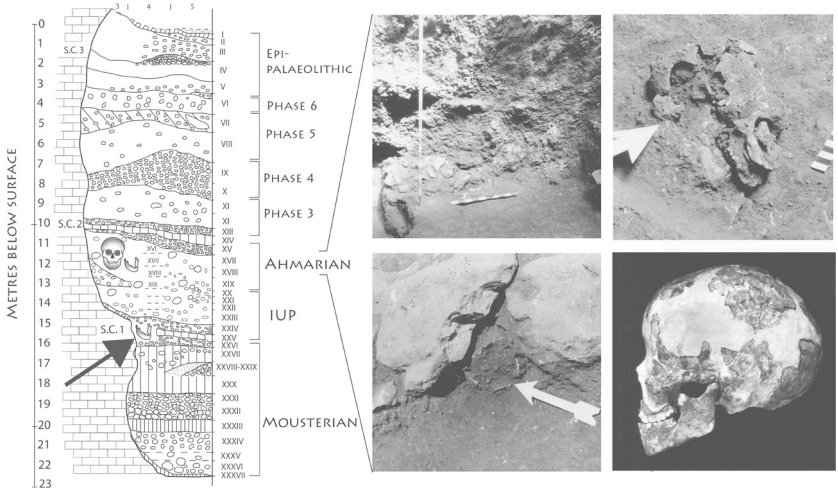

Figure 25 The stratigraphic section (left) shows the succession of archaeological layers in the site of Ksar Akil. The location of Egbert is shown (pictured right during excavation and after reconstruction). Ethelruda is shown left, arrowed in its position in the IUP.

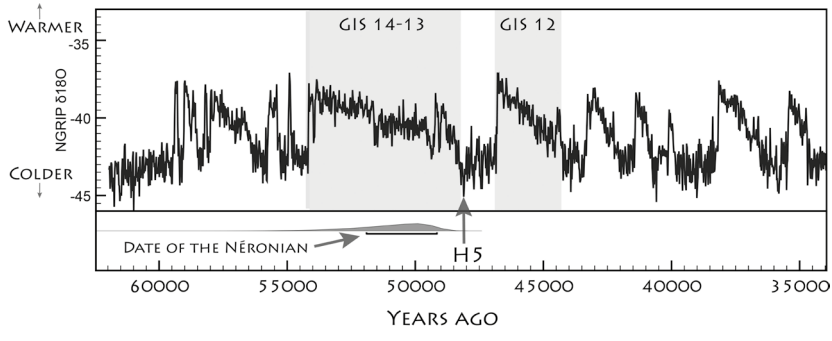

Figure 26 Comparison of the date of the Néronian modern human occupation at Mandrin with the H5 climate event about 48,000 years ago. It would be more than 4,000 years until modern humans were next seen in Europe. GIS stands for 'Greenland interstadial'; GIS-14–13 is the longest phase of warmer conditions we see during this long period of time. H5 – the Heinrich event arrowed, brings this to a shuddering halt.

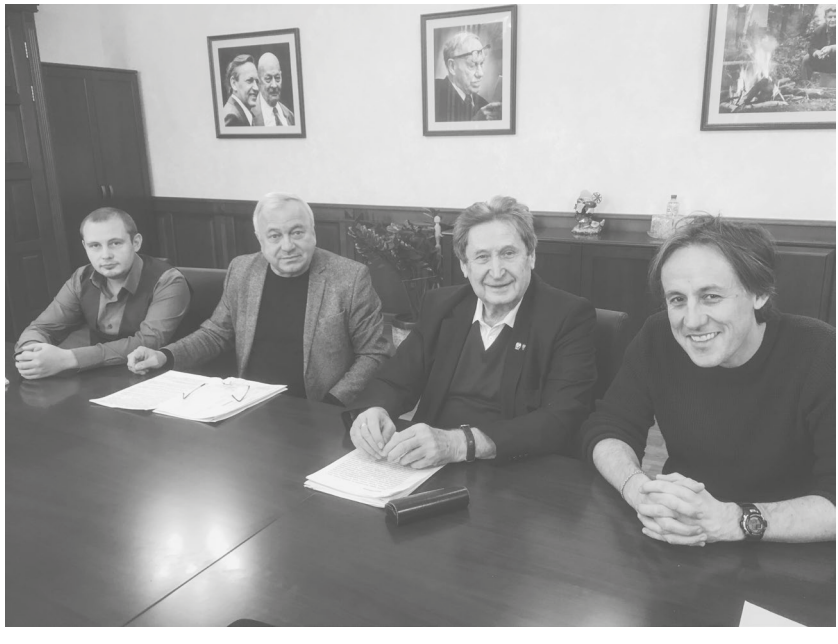

Figure 27 Meeting with (from left to right) Maxim Kozlikin, Michael Shunkov and Anatoly Derevianko in Novosibirsk. Not feeling particularly great at this point . . .

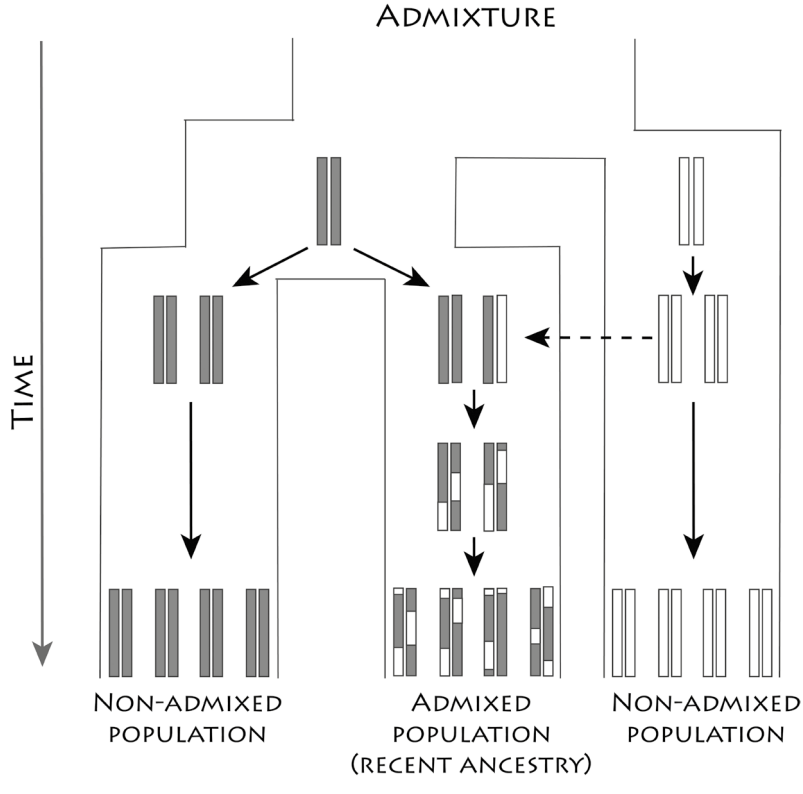

Figure 28 How admixture and recombination works. Large tracts of admixed DNA are evident closer to the introgression event when two previously separate populations interbreed. The larger the block sizes, the closer to the interbreeding event (denoted by the dashed arrow) you are.

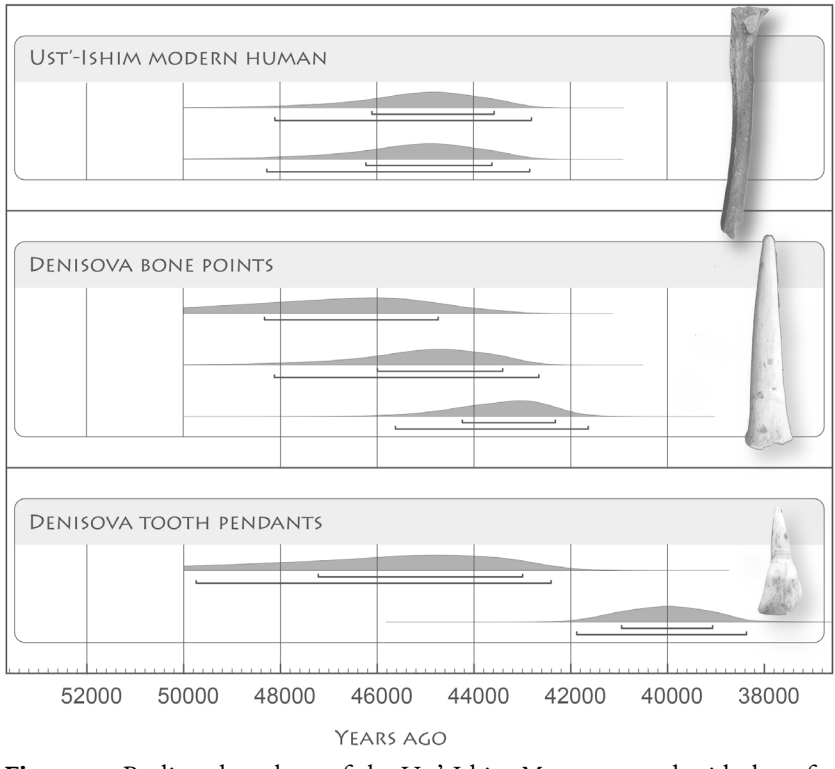

Figure 29 Radiocarbon dates of the Ust'-Ishim Man compared with dates for bone points and ornaments from Denisova Cave.

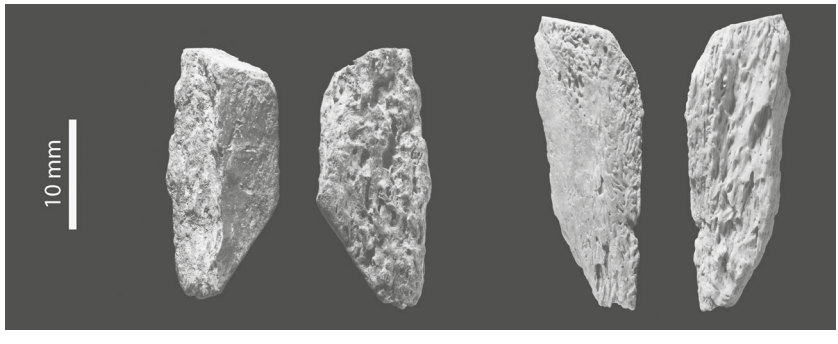

Figure 30 The two tiny bones found with ZooMS: Denisova 14 on the left and Denisova 15 on the right. Two angles for each bone are shown. These two tiny fragments were the first human bones we had found since Denny, after screening a total of more than 3,500 bone fragments.

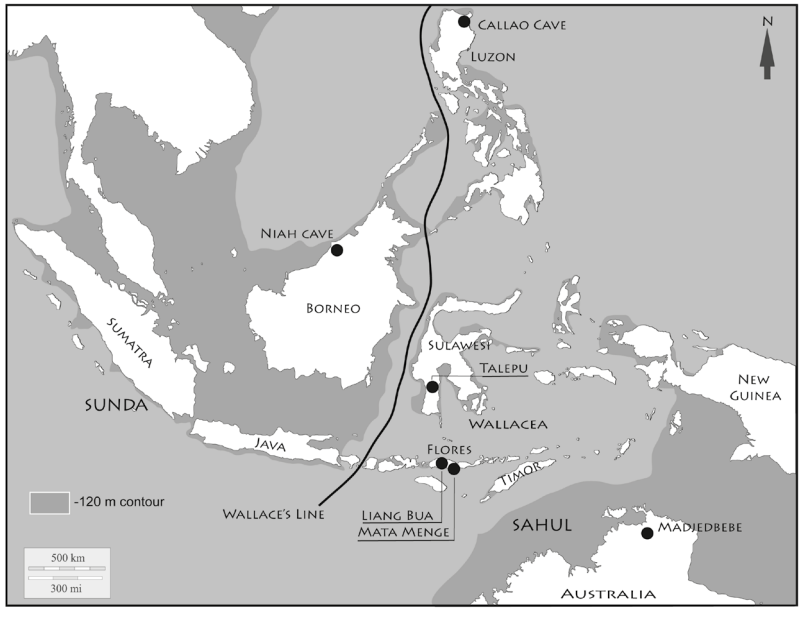

Figure 31 Sites and locations featured in this chapter. The sea levels from 30,000 to 80,000 years ago fluctuated between 50m and 120m below current levels. In this illustration the −120m contour is shown to give an idea of the maximum size of the additional landmass of Sunda and Sahul. Wallace's Line is that modified by T. H. Huxley.

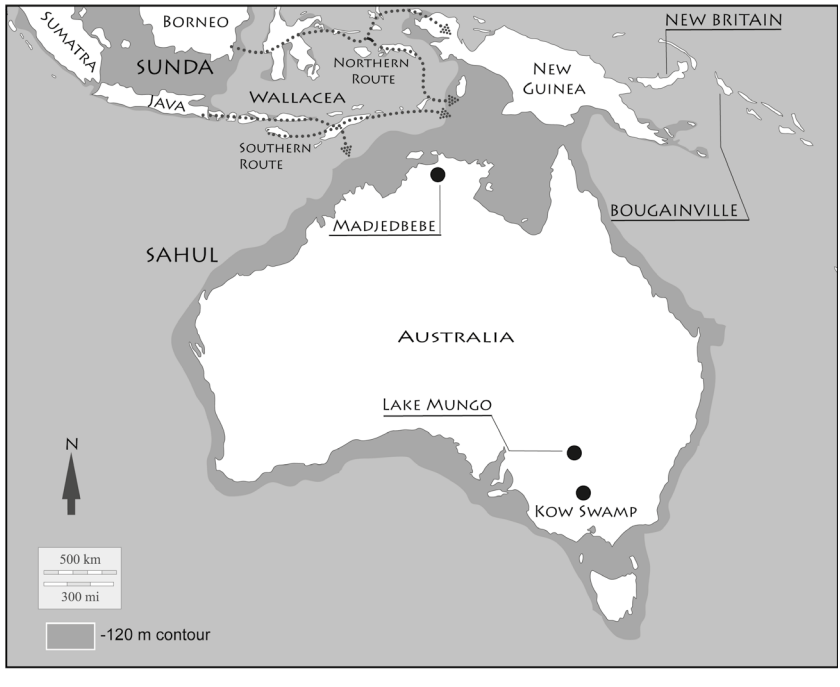

Figure 32 Sites and locations mentioned in this chapter. Note the low sea-level contour at −120m.

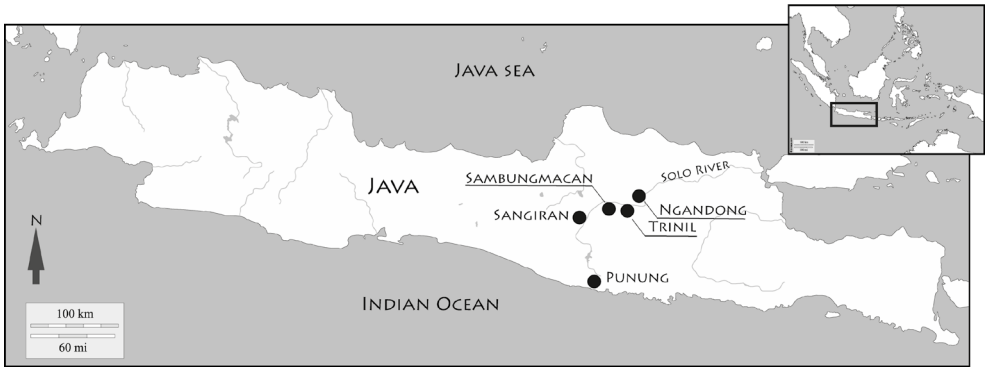

Figure 33 Sites and locations mentioned in this chapter.

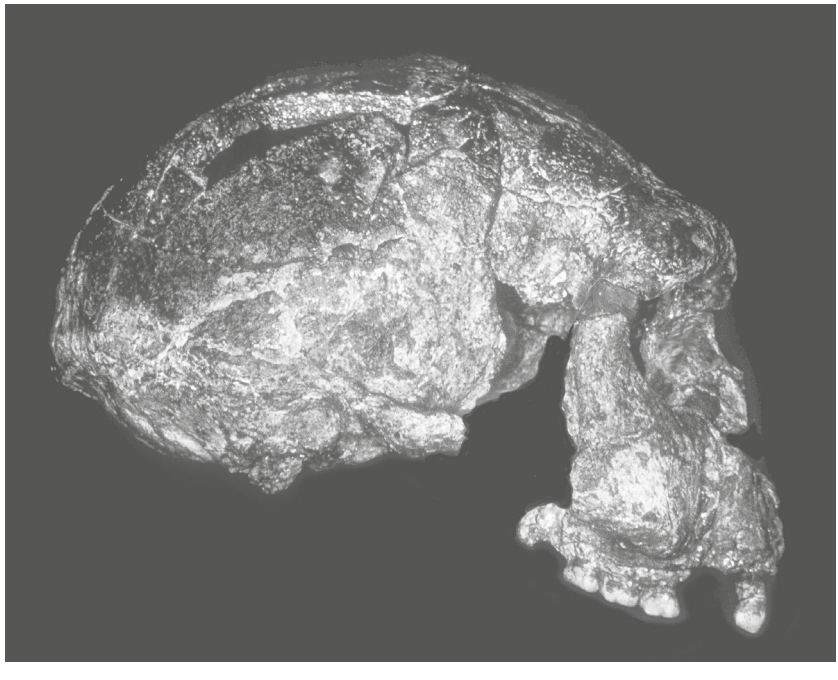

Figure 34 Sangiran 17.

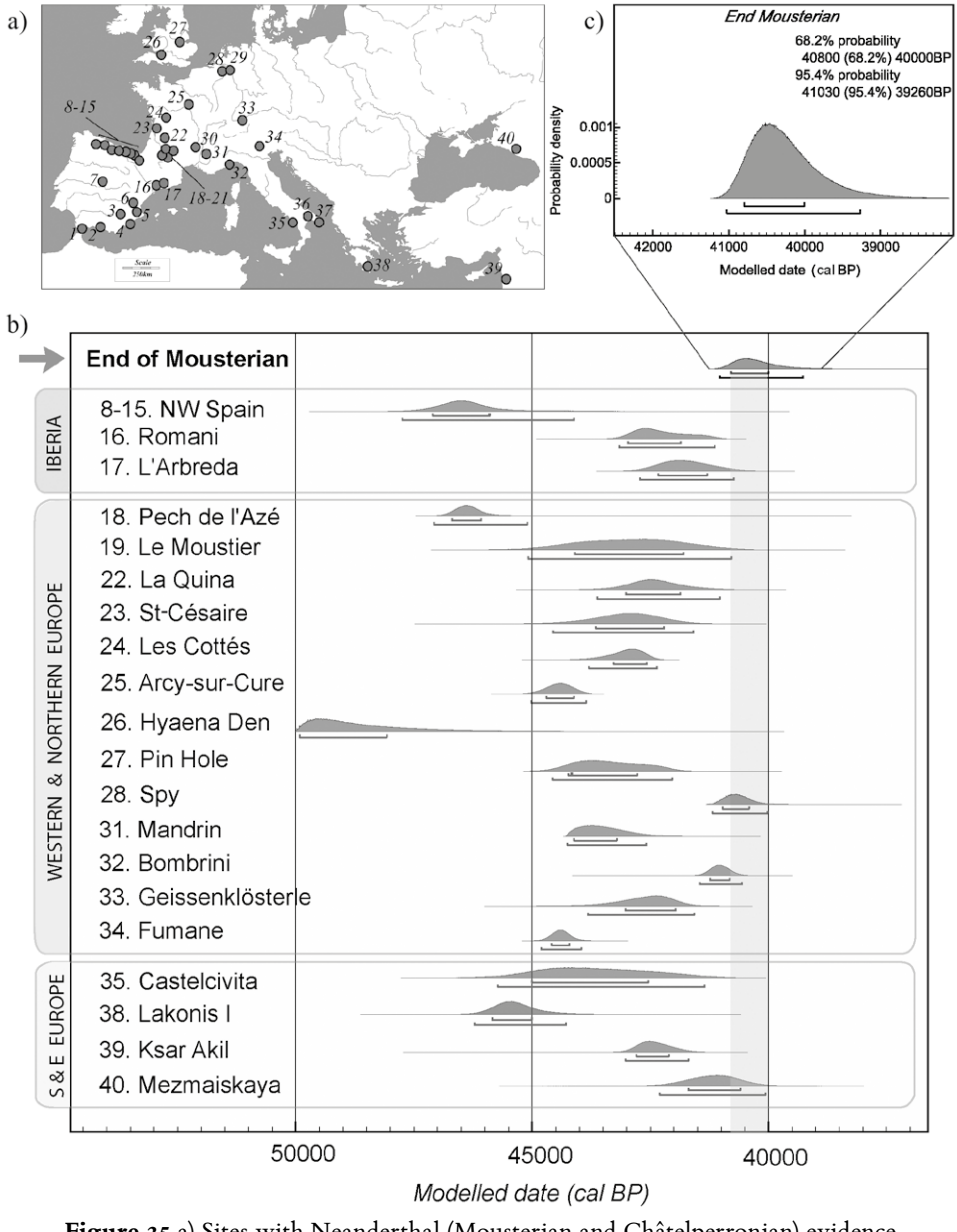

Figure 35 a) Sites with Neanderthal (Mousterian and Châtelperronian) evidence that were dated. b) The Bayesian model of the dated sites. c) The final age estimate for Neanderthal disappearance.

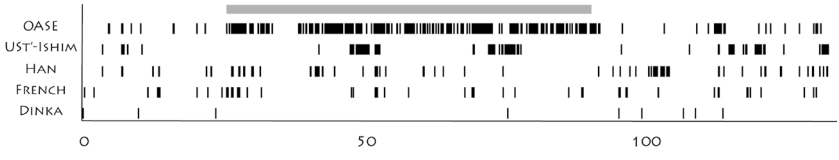

Figure 36 A section of the genome from Oase Man (top line). Black lines indicate the positions of Neanderthal-like alleles on the genome. Below Oase is Ust'-Ishim and below that three modern human genomes, a Han Chinese person, a French person and a Dinka person (from South Sudan), are shown for comparison. The grey shading at the top indicates the area of strong Neanderthal ancestry in Oase, indicating a very recent Neanderthal ancestor. This section of the genome is Chromosome 12, one of 22 chromosomes that were studied (modified after Fu et al. 2015; see note 14).

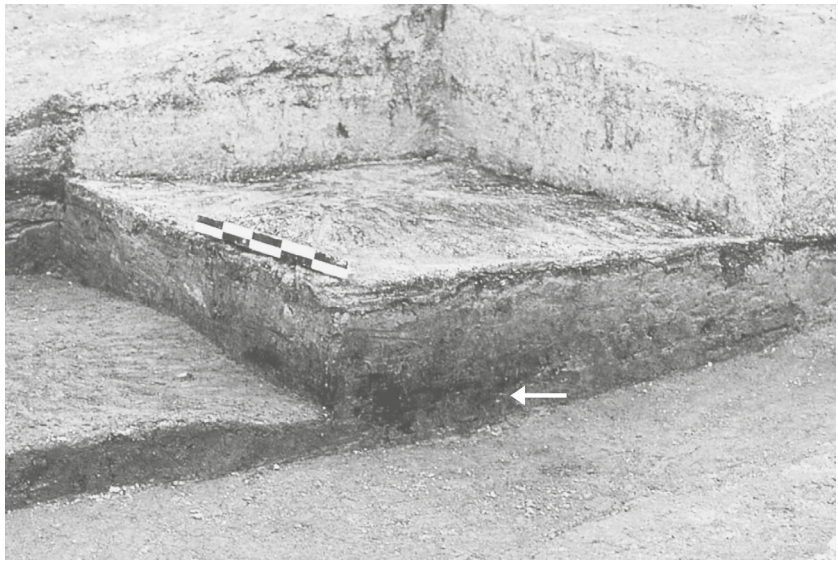

Figure 37 The Serino site. White arrow indicates an Aurignacian (early human) fireplace. Above is volcanic ash from the Campi Flegrei eruption.